 Open access • Journal Article • DOI:10.1061/(ASCE)0733-9429(1998)124:2(192)

Characteristics of Undular Hydraulic Jumps: Experiments and Analysis

— [Source link](#) 

J. S. Montes, Hubert Chanson

Published on: 01 Feb 1998 - Journal of Hydraulic Engineering (American Society of Civil Engineers)

Topics: Energy–depth relationship in a rectangular channel, Adverse pressure gradient, Hydraulic jump, Open-channel flow and Shock wave

Related papers:

- [Characteristics of undular hydraulic jumps. experimental apparatus and flow patterns](#)
- [Open channel flow](#)
- [Hydraulic condition for undular-jump formations](#)
- [Fluid mechanics for hydraulic engineers](#)
- [Characteristics of Undular Hydraulic Jumps](#)

Share this paper:    

View more about this paper here: <https://typeset.io/papers/characteristics-of-undular-hydraulic-jumps-experiments-and-1ry4zgl9pl>

CHARACTERISTICS OF UNDULAR HYDRAULIC JUMPS: EXPERIMENTS AND ANALYSIS

By J. S. Montes¹ and H. Chanson²

ABSTRACT: The writers measured velocity, pressure and energy distributions, wavelengths, and wave amplitudes along undular jumps in a smooth rectangular channel 0.25 m wide. In each case the upstream flow was a fully developed shear flow. Analysis of the data shows that the jump has strong three-dimensional features and that the aspect ratio of the channel is an important parameter. Energy dissipation on the centerline is far from negligible and is largely constrained to the reach between the start of the lateral shock waves and the first wave crest of the jump, in which the boundary layer develops under a strong adverse pressure gradient. A Boussinesq-type solution of the free-surface profile, velocity, and energy and pressure distributions is developed and compared with the data. Limitations of the two-dimensional analysis are discussed.

INTRODUCTION

The transition from a supercritical flow to a subcritical flow when the upstream Froude number F_0 is close to unity is called an undular jump. In this type of jump, the flow is characterized by free-surface undulations of decreasing amplitude (Fig. 1), which extend for a considerable distance downstream of the transition, and which replace the roller structure of the conventional jump. Undular jumps have been experimentally studied and described by many authors: Darcy and Bazin (1865), Bakhmeteff and Matzke (1936), Fawer (1937), Binnie and Orkney (1955), Ippen and Harleman (1956) as part of their study on crosswaves in supercritical flow, Ryabenko (1990), and Yasuda et al. (1993). The total extent of the available data in this type of jump is still very small and the more extensive tests performed by Chanson were described partially and analyzed by Chanson and Montes (1995) and presented in full by Chanson (1995). These experiments were supplemented by the work of Dunbabin (1996) and Lindus (1996), which concentrated on the velocity distributions in the region preceding the jump and on the shock-wave formation.

The experiments by Chanson at the University of Queensland were designed to fill some of the more obvious gaps in the subject. In Chanson and Montes [(1995) hereafter CM95] the writers noted the differences between traveling undular surges and undular jumps, and reported on the observed flow patterns of undular hydraulic jumps in a smooth rectangular channel 25 m long and 0.25 m wide. The experiments were performed with fully developed upstream shear flows in which the upstream Froude number, F_0 , ranged from 1.05 to 3.0 and the aspect ratio y_c/W varied between 0.075 and 0.455. These experiments determined centerline surface profiles, together with velocity energy and pressure distributions at selected sections along the centerline of the undular jump. These measurements were complemented with visual and photographic observations on the cross-wave geometry and the extent and position of surface rollers.

The experiments of Dunbabin (1996) and Lindus (1996) at the University of Tasmania supplement certain areas of the experimental work by Chanson. Dunbabin performed experiments in a channel of 300 mm internal width and 12 m length

with smooth Perspex walls; Lindus experimented in a 200-mm-wide similar channel. Dunbabin's experiments concerned a detailed exploration of the velocity and pressure distribution upstream of the first crest and were carried out at three different Froude numbers, $F_0 = 1.41, 1.52,$ and $1.63,$ at which the aspect ratios y_c/W of the flow were 0.247, 0.287, and 0.263, respectively. Lindus' measurements concerned the transverse velocity distribution and the onset of lateral shock wave formation. The Froude numbers of the upstream, well-developed flow were between 1.64 and 1.89, and the aspect ratios were between 0.205 and 0.225.

Possible Types of Undular Jumps

These observations indicated that five type of undular jumps could be described, according to the appearance of cross-flow (Mach) waves generated at the side walls and the formation of a surface roller at the intersection of the cross waves. Limiting values of the Froude number to separate the different states of flow were obtained through observation. These values were found to be sensitive to the aspect ratio, y_c/W , of the channel: the higher the aspect ratio, the lower the limiting Froude number for a particular class. This classification amplified the threefold classification of undular jumps suggested by Fawer in 1937. Briefly, below an upstream Froude number of 1.2 (jump type A), cross waves do not appear and the structure of the jump is nearly two-dimensional—therefore independent of the actual aspect ratio. At the upper range of possible Froude numbers (jump type E), the effect of the aspect ratio is very marked. The limit of existence of the undular jump is found at an initial Froude number of about 2.9 when $y_c/W = 0.10$, but when the aspect ratio is increased to 0.45 the Froude number is reduced to only 1.5. Beyond these Froude number values, the free-surface undulations downstream of the jump disappear and the jump reverts to a "weak" conventional jump. For low aspect ratio (<0.10) the transition Froude

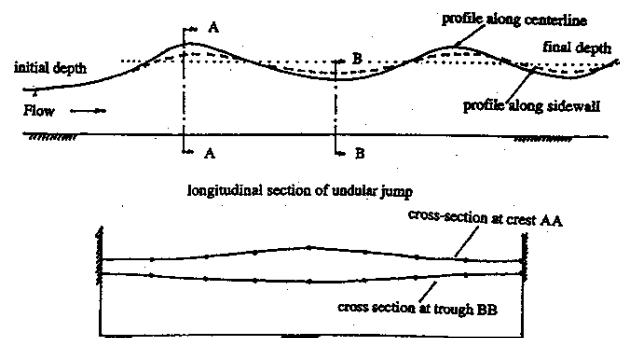


FIG. 1. Longitudinal and Transversal Cross Section of Typical Undular Jump, Showing Centerline and Wall Profiles

¹Sr. Lect., Dept. of Civ. and Mech. Engrg., Univ. of Tasmania, Hobart TAS 7050, Australia.

²Sr. Lect., Hydr. and Fluid Mech., Dept. of Civ. Engrg., Univ. of Queensland, Brisbane QLD 4072, Australia.

Note. Discussion open until July 1, 1998. To extend the closing date one month, a written request must be filed with the ASCE Manager of Journals. The manuscript for this paper was submitted for review and possible publication on March 4, 1997. This paper is part of the *Journal of Hydraulic Engineering*, Vol. 124, No. 2, February, 1998. ©ASCE, ISSN 0733-9429/98/0002-0192-0205/\$4.00 + \$.50 per page. Paper No. 7841.

numbers for the different undular jump types were found to be:

- Type A: No cross waves, two-dimensional structure, $F < F^A = 1.22$
- Type B: Cross waves develop, but there is no wave breaking at their intersection, $F < F^B = 1.72$
- Type C: Wave breaking can be detected at the first cross-wave intersection, small roller, but no air entrainment, $F < F^C = 2.10$
- Type D: Air entrainment is noticeable at the intersection of the cross waves on the first crest, $F < F^D = 2.40$
- Type E: The roller formed at the first cross-wave intersection widens, undulations disappear, $F < F^E = 2.6$

This paper presents additional observations on the measured distributions of pressure, velocity, and energy and their comparison with the numerical solution of a two-dimensional Boussinesq model of the undular jump. This comparison has the purpose of defining clearly the applicability of this type of solution to the undular jump.

EXPERIMENTAL RESULTS

A large number of experiments were performed to record the free-surface profiles on the centerline. Some experiments (shown in Table 1, first eight performed by Chanson and last three by Dunbabin) included measurements of velocity, pressure, and total head distributions at the jump centerline at various locations along the undular jump: i.e., upstream of the jump (U/S), at the centerline of the lateral shock waves (SW), at the first crest (1C), at the first trough (1B), at the second crest (2C) and trough (2B), and at the third crest (3C). A full presentation of the data in the first eight runs can be found in Chanson (1993).

Fig. 2 presents a typical set of free-surface profiles on the centerline. As commented in CM95, when the undular jump has an initial Froude number greater than 1.2 (undular jump type B to E), the transversal water-surface profile is not horizontal, but the transversal profile has the maximum rise and depression at the centerline, while the longitudinal surface profile at the side wall has a much attenuated wave amplitude. The structure of the jump is markedly three-dimensional, with perceptible changes in the distribution patterns of velocity, energy, and pressure across the flow. A plan view of the jump (types B to E) would show a diamond pattern of the surface, caused by the reflection of the cross waves on the vertical walls of the channel, while the surface topography would be dominated by the symmetrical hills at the crests and by the valleys at the troughs of the wave.

TABLE 1. Summary of Velocity and Pressure Distribution Experiments

Run (1)	q (m ² /s) (2)	y_c/W (3)	h_1 (m) (4)	F_0 (5)	Slope (6)	Type of undular jump (7)
HMTJ1	0.0198	0.137	0.0292	1.27	0.0044	B
HMTJ2	0.0198	0.137	0.0240	1.70	0.0083	C
HMTJ5	0.0200	0.138	0.0210	2.10	0.0132	D
HMTJ6	0.0198	0.137	0.0191	2.40	0.0173	E
HMTJ3	0.0397	0.217	0.0468	1.25	0.0044	B
HMTJ7	0.0399	0.218	0.0420	1.48	0.0038	C
HMTJ4	0.0400	0.219	0.0384	1.70	0.0083	D
TT2_1	0.0598	0.286	0.0456	1.35	0.0049	B
RD_1	0.0631	0.247	0.061	1.41	0.003	B
RD_2	0.0792	0.287	0.067	1.52	0.003	B
RD_3	0.0695	0.263	0.057	1.63	0.003	B

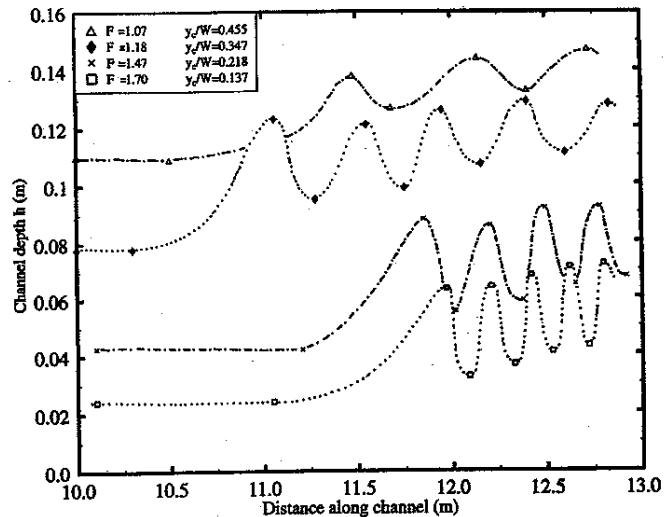


FIG. 2. Typical Centerline Free-Surface Profiles of Undular Jumps, $W = 0.25$ m (Chanson 1993)

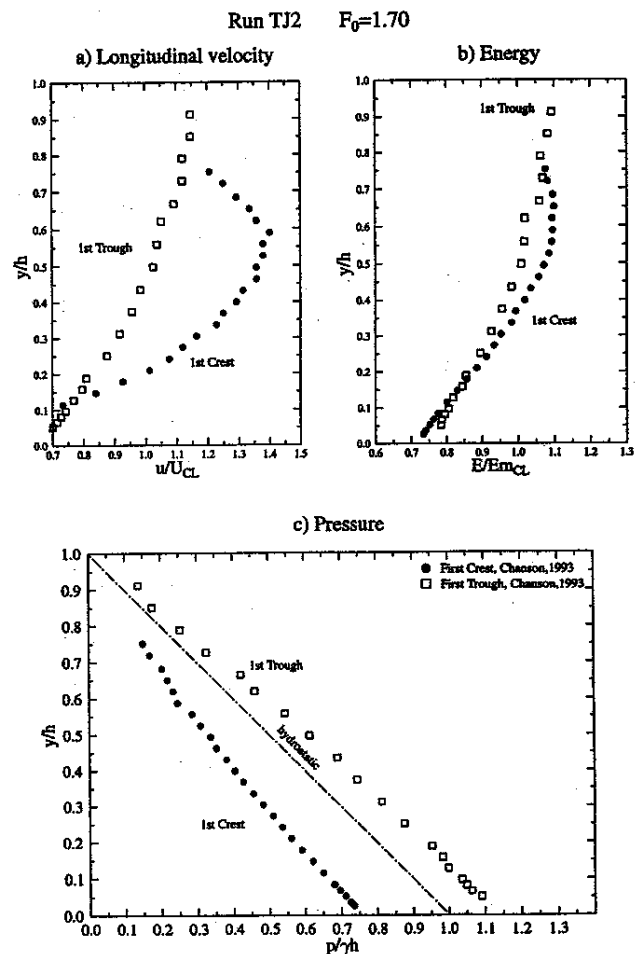


FIG. 3. Dimensionless Velocity u/U_{CL} , Specific Energy $E/(E_m)_{CL}$, and Pressure $p/(\gamma h)_{CL}$ Distributions along Centerline (Undular Jump Type D), Run TJ2 $F_0, y_c/W = 0.138$

Velocity, Energy, and Pressure Distributions

Fig. 3 shows experimental velocity, energy, and pressure data for a typical run (HMTJ2 in Table 1), at locations under the first crest and the first trough. The velocities, Fig. 3(a), were normalized by the mean centerline velocity U_{CL} , and shown as a function of y/h , where y = distance from bed mea-

sured normal to channel bottom, and h = centerline flow depth. Fig. 3(b) shows the dimensionless specific energy, $E/(E_m)_{CL}$, as a function of y/h . The local specific energy, E , is the energy per unit weight with elevation datum taken as the bottom of the channel, and $(E_m)_{CL}$ is the mean specific energy on the centerline. The pressure distribution [Fig. 3(c)] is presented as $p/(\gamma h \cos \phi)$ versus y/h , where p = pressure; and ϕ = slope angle of bottom.

Fig. 3 shows a major change of the velocity profile between the upstream flow and the first wave crest. In particular, a strong velocity decrease is observed near the free surface for all but the lowest Froude numbers. Indeed, for $F_0 > F^B$ (see Introduction), a wave-breaking (roller) and air bubble entrainment take place at the free surface (CM95). The process enhances the energy dissipation at the free surface and causes a local velocity reduction.

Downstream of the first wave crest, the velocity field at the first trough has a shape similar to the upstream flow. At the start of the shock waves, the velocity profile diverges only slightly from the upstream velocity field.

Three-Dimensional Nature of Flow Field within Undular Jump

The three-dimensional nature of the flow is attested by Figs. 4(a) and 4(b), which show Lindus's (1996) experiments in a 200-mm-wide perspex rectangular channel at the University of Tasmania. The velocity profiles at the 1C location show not only the expected reduction of the mean value, but also that the profiles are dissimilar, with a lowering of the point of maximum velocity and a further reduction of the surface velocity toward the wall.

Another indication of the three-dimensional nature of the flow in the undular jump is given by the variation of the mean velocity along a vertical plane. The integration of the velocity measurements on the centerline shows consistently that the centerline discharge, $(q)_{CL}$, is larger than the mean discharge unit discharge, $q = Q/W$, and oscillates along the jump.

$$(q)_{CL} = \int_0^h u \, dy \quad (1)$$

In Fig. 4c, the centerline discharge of the Chanson experiments summarized in Table 1 is presented as a function of the location along the jump. It shows that larger centerline discharges are observed at the crests than at the wave troughs, as is to be expected in light of the strong deceleration that the flow suffers near the crest sections (Figs. 3a and 4a), which tends to emphasize the velocity differential with the flow near the wall. The acceleration observed near the troughs explains the greater uniformity of the integrated discharge at trough sections 1B and 2B. As the pressure gradients that control the flow acceleration increase with the Froude number of the flow, it is reasonable to connect the oscillation of $(q)_{CL}$ to the Froude number. For the experiments reported in Table 1, the dimensionless centerline discharges $(q)_{CL}/q$ range between 1.05 and 1.6 at the wave troughs, and from 1.1 to 2.05 at the wave crests. Hager and Hutter (1984) found a similar longitudinal fluctuation of the ratio $(q)_{CL}/q$, although of smaller magnitude than that found in the present experiments. The fact that the boundary layer was not fully developed before the jump in their experiment may account for this difference.

Normalization of Velocity Profiles in Region Preceding Jump

Dunbabin (1996) conducted a special study of this velocity distribution in this region. Dunbabin measured the centerline velocity distribution at several locations from the beginning of

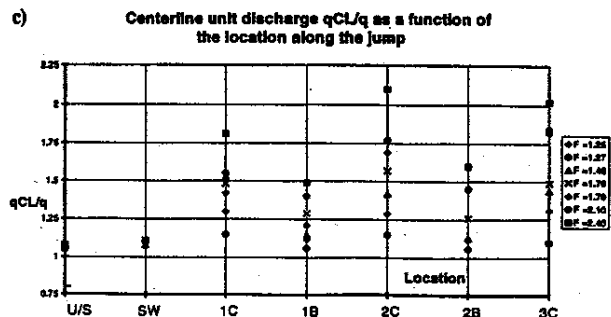
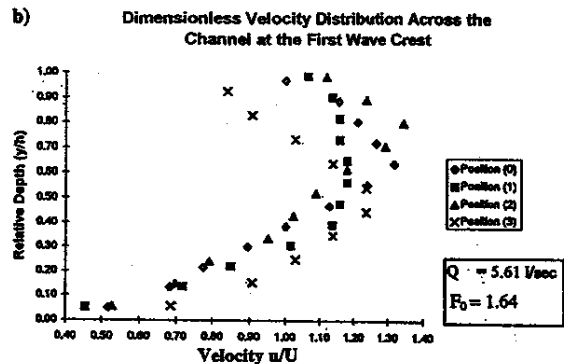
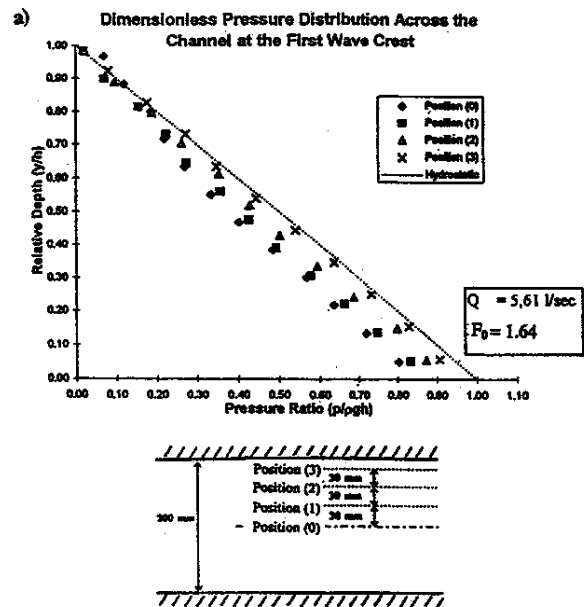


FIG. 4. Three Dimensional Effects in Undular Jump: (a) Pressure Distributions at Four Transversal Locations. Curvature Effects Seem Much Weaker Near Wall, Data from Lindus (1996); (b) Velocity Distributions at Same Locations, with More Uniform Profile near Wall, Data from Lindus (1996); (c) Centerline q_{CL}/q Discharge Distribution at Selected Locations, Data from Chanson (1993)

the jump to the second crest. The findings are that in these zones of large, initially adverse and then favorable pressure gradients, the velocity distributions have an inner region that obeys the law of the wall (logarithmic velocity distribution)

$$\frac{u_{inner}}{u_*} = \frac{1}{K} \ln \left(\frac{y u_*}{\nu} \right) + B \quad (K \approx 0.4, B \approx 5.5) \quad (2)$$

and an outer region that complies with Coles' "law of the wake"

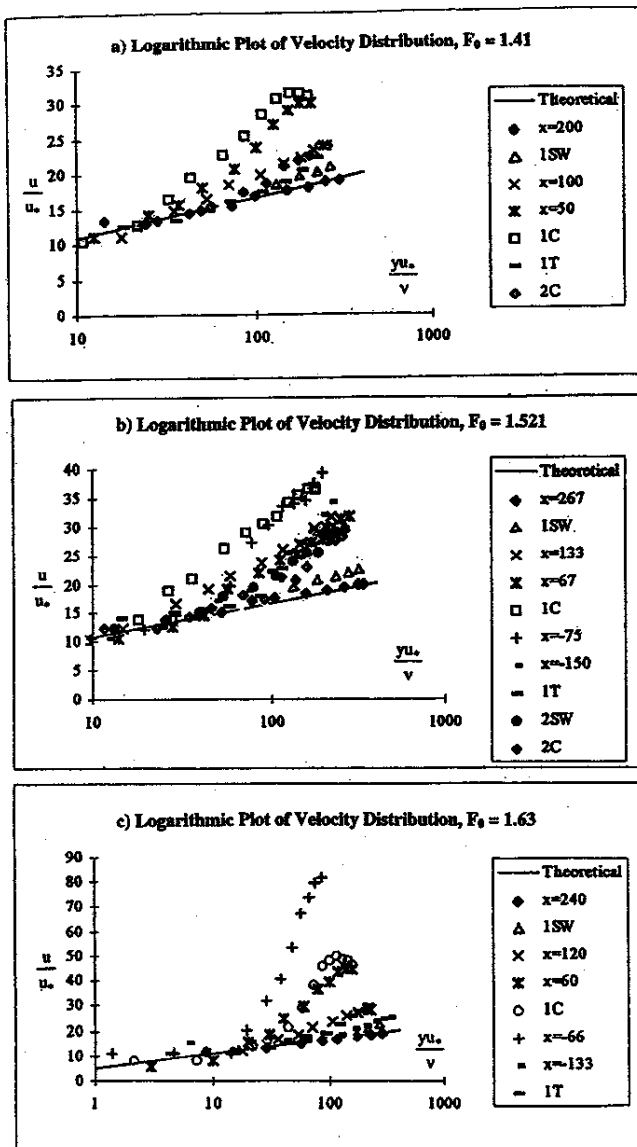


FIG. 5. Log Plot of Velocity Distribution, Showing Deviation from "Law of the Wall" Due to Adverse Pressure Gradient as Crest Location Is Approached (Dunbabin 1996)

$$\frac{\Delta u}{u_*} = \frac{\Pi}{K} \omega \left(\frac{y}{h} \right) \quad (3)$$

The shape $\omega(y/h)$ of the outer region, as found experimentally by Coles, has a characteristic S shape, and is such that $\omega = 0$ for $y/h = 0$ and $\omega = 2$ for $y/h = 1$. This shape is closely approximated by the function

$$\omega \left(\frac{y}{h} \right) = 1 + \sin \left[\frac{\pi}{2} \left(2 \frac{y}{h} - 1 \right) \right] \quad (4)$$

Fig. 5 shows velocity profiles at the centerline for $F_0 = 1.41$, 1.52, and 1.63. The trend of the experimental points in Dunbabin's experiments follows the normalized wake function of Coles, as seen in Fig. 6a, which shows the results for $F_0 = 1.41$. The magnitude of the wake component, which is defined by Coles' parameter, Π , also varies considerably along the undular jump, in response to the variable pressure gradient. It is at maximum just below the first crest (Fig. 6b), but by the second crest it has returned to a value of about half the maximum, showing the effect of a smaller adverse pressure gradient. Dunbabin correlated the magnitude of the amplitude pa-

rameter, Π , with the nondimensional longitudinal pressure gradient parameter, $\beta = (h/\tau_b)/(dp/dx)$, approximated here by the expression $\beta = (gh/u_*^2)/(dh/dx)$. This correlation, which covers a very wide range of values of the pressure gradient parameter, is shown in Fig. 6c. The experimental trend is approximated by the empirical curve defined by

$$\Pi = 0.2\beta^{0.5} \quad (5)$$

which applies only to the positive values of β . The undular jump data points follow the same trend as other cases derived from the extensive experimental database reported by Coles and Hirst (1968). The only other available free-surface flow experiments that supplied data for Fig. 6c, those of Kironoto and Graf (1994), have comparatively small pressure gradients.

Pressure Distributions

The pressure measurements on the channel centerline [shown in Fig. 3(c) and 4(b)] indicate that the pressure distri-

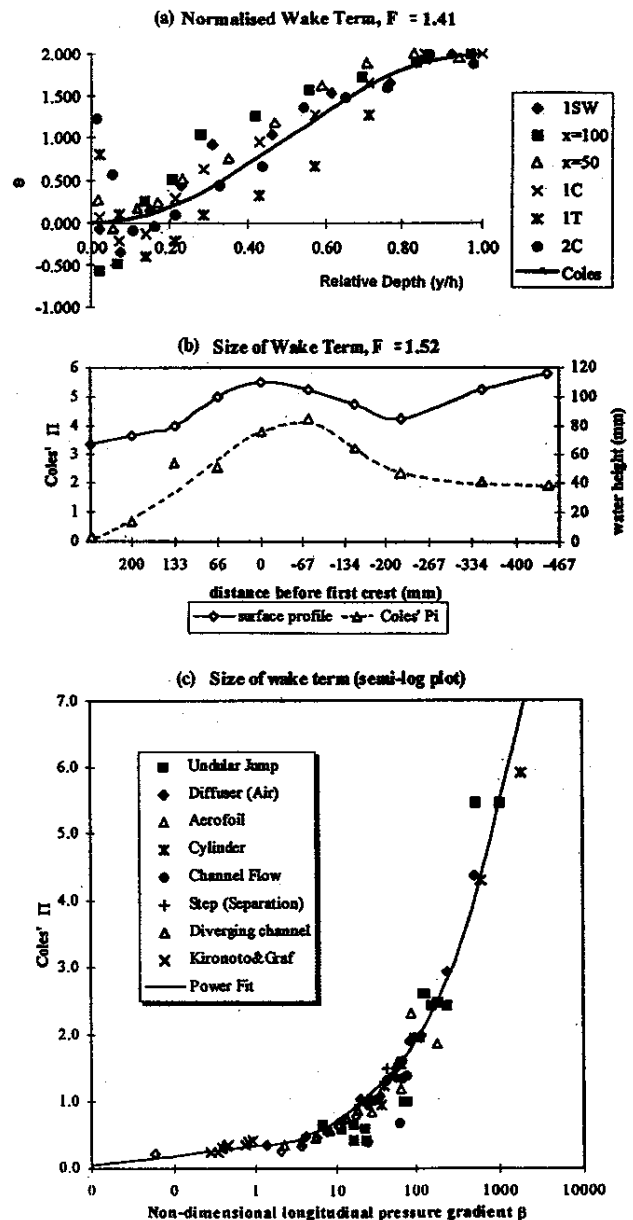


FIG. 6. From Dunbabin (1996) at $F_0 = 1.41$: (a) Experimental Wake Profile Is Similar to Coles' Profile; (b) There Is a Lag in Minimum and Maximum of Wake Amplitude with Respect to Crest and Trough Locations; (c) Wake Amplitude Correlates Well with Pressure Gradient β

bution along the undular jump is not hydrostatic. At each wave crest, the pressure gradient dp/dy is less than the hydrostatic pressure, and at each wave trough, the pressure gradient is larger than the hydrostatic pressure. This behavior is predicted by the Boussinesq equation type of solution discussed in the analysis section and is also a well-known result of elementary wave theory.

Chanson's (1995) experimental data indicate that the depth-averaged pressure gradient $(dp/dy)_{av}/(\gamma \cos \phi)$ is a function both of the position along the jump and of the upstream Froude number. Two aspect ratios were used in this calculation: $AR = 0.137$ and $AR = 0.218$. The results indicate that the mean pressure gradient on the centerline may differ by up to 20% from the hydrostatic gradient value (i.e., -1); the maximum difference is observed at the first wave crest (1C). The deviation of the mean pressure gradient from hydrostatic conditions decreases along the jump from the first crest (1C) to the third crest (3C) and from the first trough (1B) to the second trough (2B). The results also show that the deviations from the hydrostatic pressure increase as the aspect ratio decreases.

Yasuda et al. (1993) recorded bottom pressures along an undular jump downstream of a gate. The upstream flow was a partially developed boundary layer flow. A comparison between Yasuda et al.'s data and the writers' data (of similar Froude number and aspect ratio) indicates the same trends for both experiments, although larger pressure gradient fluctuations were observed by Yasuda et al. This result suggests that the upstream flow conditions affect the amplitude of the pressure gradient along the jump.

Energy Dissipation on Centerline

A situation observed in the undular jump closely parallels a well-known phenomenon in aerodynamics. This is the large change in the fluid drag if the Froude number (Mach number in compressible flow) is increased slightly above the critical flow value. The rise in profile drag, for example, is exceptionally acute on an aerofoil as the Mach number increases beyond 0.8. The beginning of the undular jump is precisely in this region of "transcritical" flow (transonic flow in aerodynamics). The experiments show consistently that most of the energy dissipation along the centerline takes place between the start of the lateral shock waves (SW) and the first crest (1C). Downstream of the first crest, the head loss gradient $-\Delta H/\Delta x$ is of the same order as the bed slope $\sin \phi$. This fact had also been observed by Fawer (1937). In Fig. 7 the energy dissipation on the centerline, $(\Delta H)_{CL}$, between the upstream flow (U/S) and 1C is plotted as a function of the upstream Froude number, where $(\Delta H)_{CL} = \text{head difference}$

$$(\Delta H)_{CL} = (H)_{US} - (H)_{1C} \quad (6)$$

and $H = \text{total head at the centerline}$. The experimental data of Fig. 6 are compared with the theoretical energy loss, ΔH , in the jump from one-dimensional momentum equation

$$\frac{\Delta H}{y_c} = \frac{(\sqrt{1 + 8F_1^2} - 3)^3}{16F_1^{2/3}(\sqrt{1 + 8F_1^2} - 1)} \quad (7)$$

Fig. 7 suggests that the equation underestimates the energy dissipation on the centerline even for the smallest Froude numbers.

At the start of the shock waves, the pressure distribution is quasi-hydrostatic and the velocity profile is close to the upstream velocity field. A comparison with the velocity and pressure distributions at the first crest (Figs. 3a and 3c) shows that a major flow redistribution occurs between the start of the shock waves and the first crest. Most of the energy is then dissipated in association with the modification of the pressure

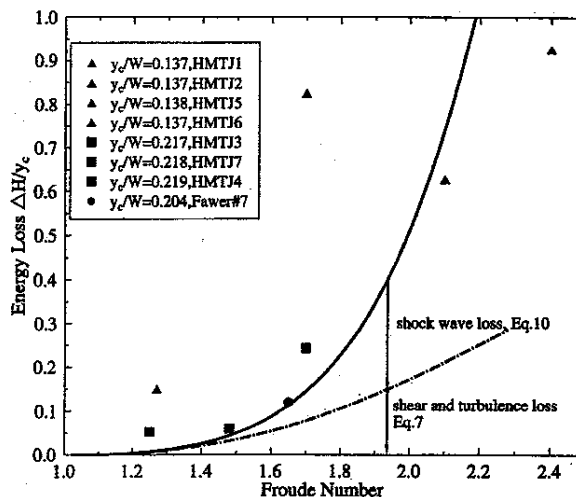


FIG. 7. Energy Dissipation along Centerline between Upstream Section and First Crest. Dissipation is in Excess of That of Conventional Jump, a Difference Attributed to Additional Drag Due to Lateral Shock Waves

and velocity fields, which are markedly three-dimensional in this region. Because of this characteristic, the centerline measurements are representative but do not necessarily fully describe the entire flow field.

SHOCK WAVES IN UNDULAR JUMP

Shock waves first form just downstream of the beginning of the undular jump, and once formed they are reflected from the side walls until they encounter wholly subcritical flow conditions. The formation of the shock waves is in itself paradoxical. In transonic flow, shock waves' existence is associated with the existence of a body with surface discontinuities; in hydraulics, with changes of alignment of the channel walls. Obviously such conditions are not met here. The idea is advanced here that the shock waves form due to the rapid growth of the boundary layer on the side walls caused by the adverse pressure gradient at the beginning of the jump. The supercritical flow regards the solid boundary of the side wall as being displaced inward by the lateral boundary layer, and when the side-wall boundary layer thickens appreciably due to the adverse pressure gradients and eventually separates from the wall, the shock waves start. The "body" shape needed for the formation of the shock waves is the virtual boundary created by the boundary layer's separating from the solid wall. Once formed, the shock waves propagate across the flume and restore the momentum equilibrium by means of this displacement. The increase in drag is then predominantly a wave drag, since the skin friction near the region of separation is very small. It follows from this argument that, unless the requisite adverse pressure gradient exists to trigger the side-wall separation, such shock waves cannot form. Flows at Froude numbers less than 1.2 do not have the necessary rise in the water-surface profile up to the first crest to generate the gradient.

Lindus (1996) conducted experiments of a qualitative nature to test this hypothesis. By using a thread as a tracer near the wall, Lindus observed that the thread fluctuated and separated perceptibly near the start of the shock waves, although at locations upstream of this point, it remained aligned with the wall. In the region between the start of the shock wave and the first crest, the side-wall boundary layer remains separated and it is not until the location of the first crest has been passed that the tracer aligns itself with the wall in the accelerated region preceding the first trough. Chanson (1993) observed the presence of a vertical vortex at the junction of the shock wave with the wall; the vortex seems to stretch horizontally along

the bottom corner following the flow direction. The vortex structure is quite difficult to observe because the surface of the flow is not transparent after the start of the shock wave, but the vortex fits well with the notion of a dividing streamline of $u = 0$ rolling up at the point of separation.

The combined action of boundary-layer growth and shock-wave formation is equivalent to an additional drag force on the channel, caused by the degradation of momentum near the solid wall and the dissipation of energy across the shock wave. The first effect prevails at lower Froude numbers, and the energy radiation due to the oblique wave predominates at the upper values of the Froude number. The theory of shock-wave formation in open channels [Ippen (1951), Engelund and Munch-Petersen (1953)] finds that the angle of the shock wave to the side wall should decrease with the Froude number of the flow ($\sin \theta^* \approx 1/F_0$, for small wall-deflections). However, Chanson's (1995) experimental data suggest that this trend is not confirmed, and that the angle θ^* formed by the shock wave and the side wall remains relatively constant at a value between 37° and 40° , with a weak dependence on the aspect ratio (Fig. 7). Ippen's theory predicts that this shock wave angle would be produced in ideal fluid flow by a local-flow Froude number of $F \approx 1.7$. The divergence of the experimental result from the shock-wave formation theory may be ascribed to the interaction between the shock wave and the lateral boundary layer. The adverse pressure gradient on the boundary layer increases with the Froude number because of the increased depth ratio between the upstream position and first crest position. The lateral boundary layer consequently thickens and eventually separates near the point of shock-wave formation. Thus, it is conjectured that an equilibrium is reached, in which increases in the upstream Froude number do not increase necessarily the flow velocity at the point of inception of the shock wave, with the result that θ^* remains constant with increasing F_0 .

Drag Due to Shock Waves

An expression for the additional drag due to shock waves may be suggested by analogy with transonic drag in aerodynamics. The drag due to shock-wave formation in compressible flow can be expressed by the relation derived by C. N. Lock (Hilton 1952).

$$\text{Drag force} \propto \frac{1}{2} \rho U^2 (M_a - M_b)^4 \quad (8)$$

M = Mach number for compressible flow; M_a = starting Mach number for transonic effects; ρ = density; and U = mean speed of the flow. This equation may be recast in a form suitable for open-channel flow by using the analogy between Mach number for compressible flow and Froude number for free-surface flow (Liggett 1994). By assuming that the critical Froude number for the channel (Froude number below which shock waves cannot form is equal to 1) and introducing a coefficient of proportionality C , one finds that

$$\text{Drag force} = C \frac{1}{2} \rho U^2 (F_r - 1)^4 \quad (9)$$

To modify this relation to a form suitable for comparison with data of Fig. 8, the energy loss ΔE may be set equal to $\Delta E = S_f L$, where L = longitudinal distance between the formation of shock waves and their first crossing, and S_f = slope of the energy line. The value of L is related to the cross-wave angle θ^* and the width W of the channel: $L = W/(2 \tan \theta^*)$. The variable S_f is connected with the boundary drag through the uniform flow relation $S_f = D/\gamma h$. Using (9) for D one finds

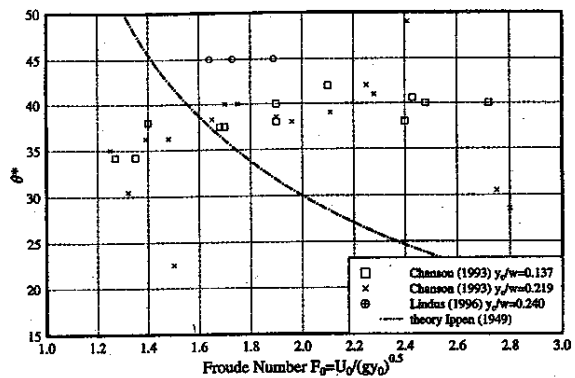


FIG. 8. Shock Wave Angle θ^* as Function of Upstream Froude Number. Comparison with Ippen's (1951) Theory

$$\Delta E = C \frac{U^2}{2gh} \left(\frac{W}{2 \tan \theta^*} \right) (F - 1)^4$$

This is equivalent to

$$\frac{\Delta E}{y_c} = \left(C \frac{\cot \theta^*}{y_c/W} \right) F_1^{4/3} - 1)^4 \quad (10)$$

The total energy loss from the beginning of the undular jump to the first crest consists of the shear and turbulence loss, which may be approximately accounted by (7), and the shock-wave loss (10). Fig. 8 suggests that the loss predicted by (10) follows the experimental trend, and that the first term on the right-hand side of (10) has a value of about 0.135. The shock-wave loss exceeds the shear losses for Froude numbers larger than 1.8, and their combined value (which is much larger than in the conventional jump at the same F_0) dispels the notion that undular jumps are phenomena almost unaffected by real fluid effects (the undular bore analogy).

ANALYSIS

The surface profile, amplitude, and wavelength of wavy flow have been predicted in the past by two-dimensional models based on the integration of the differential momentum and continuity equations (Boussinesq 1871; Fawer, 1937; Serre 1953). Although some characteristics of the undular jump are not constant across the width of the channel, as detailed in previous sections, a 2D model provides a useful, if approximate, account of the principal features of the jump and allows an understanding of one of its important features—namely, the linkage of the length and amplitude of the undulations with the energy (or momentum) balance of the flow. This model would be primarily suitable to undular jumps of type A, and perhaps of type B, but its use in the other types of jumps occurring at higher Froude numbers is questionable, since this model is limited to moderate curvatures and surface slopes.

Boussinesq (1871, 1877) was intrigued by the phenomenon of the undular jump, which had been described experimentally by Bazin (1865). Boussinesq analyzed this problem and devised a relatively simple and powerful method to integrate the 2D equations of motion for steady flow, a method that has been followed by many researchers. Boussinesq simplified the integration of the equations of motion by adopting certain plausible assumptions on the distribution of vertical and horizontal velocities, so that a single ordinary differential equation linking the flow depth and the longitudinal abscissa x is obtained. Boussinesq's original hypotheses were: (1) the horizontal velocity at any depth is equal to the mean velocity, q/h ; and (2) the vertical velocity has linear variation from the surface down. Because the surface vertical velocity is a function of the water-surface slope, the integrated energy or mo-

momentum equation contains terms related to the curvature and slope of the water surface. This extended momentum equation and similarly derived extended energy equation are called the Boussinesq equations. Fawer (1937), Serre (1953), Matthew (1963), and Hager and Hutter (1984) have used alternative closure hypotheses on different pairs of kinematic variables to integrate the momentum equations and create extended equations.

Modified Boussinesq Equation

Because the velocity distributions that follow from these closure hypotheses do not reflect adequately the effect of the developing boundary layer preceding and encompassing the undular jump, a two-part velocity distribution model is presented here. In the first part, an inviscid velocity distribution model based on fairly simple closure hypotheses is constructed. This model is later modified to account for boundary shear effects. Because of the limitations of the two-dimensional analysis of a phenomenon that has so many three-dimensional features, the model has been deliberately made as simple as possible.

Velocity Distribution in Flow with Surface Curvature

The inviscid velocity distribution analysis is based upon a streamlined centered *s-n* system, defined in Fig. 9(b), and embodies the following two geometrical assumptions:

1. The radius of curvature of the streamlines *R* between the surface and the bottom varies with the depth according to the interpolation equation

$$\frac{1}{R \cos \theta} = \frac{1}{R_b \cos \theta_b} + \left(\frac{1}{R_s \cos \theta_s} - \frac{1}{R_b \cos \theta_b} \right) \left(\frac{y}{h} \right)^K \quad (11)$$

where *K* = a positive constant of order of unity; θ = angle formed by streamline with bottom of channel at origin of *s-n* system, located a distance, *y*, from bottom; and *h* = local surface depth. The subscripts *b* and *s* define conditions at the bottom and surface of the flow.

2. The envelope of the normals to the streamlines is an arc of a circle.

By means of these assumptions it is possible to derive expressions for the streamline, longitudinal, and transversal velocity distributions and the pressure distribution [(see Appendix I and Fig. 9(b)]. These relations are derived on the assumption that the curvature and slope parameters defined by

$$\epsilon_0 = \frac{h}{R_s \cos \theta_s} = \frac{hh'}{1+h'^2} \quad (12)$$

and

$$\epsilon_1 = \frac{h'^2}{1+h'^2} \quad (13)$$

are small in comparison with unity, so their squares and products are negligible. Here the primes denote differentiation with respect to *x*.

When these expressions for the velocity and pressure distribution, which contain terms involving the surface slope *h'* and curvature *h''*, are inserted in the definitions of the mean energy and momentum (see Appendix I), we obtain the inviscid Boussinesq equations for energy and momentum (extended energy and momentum equations).

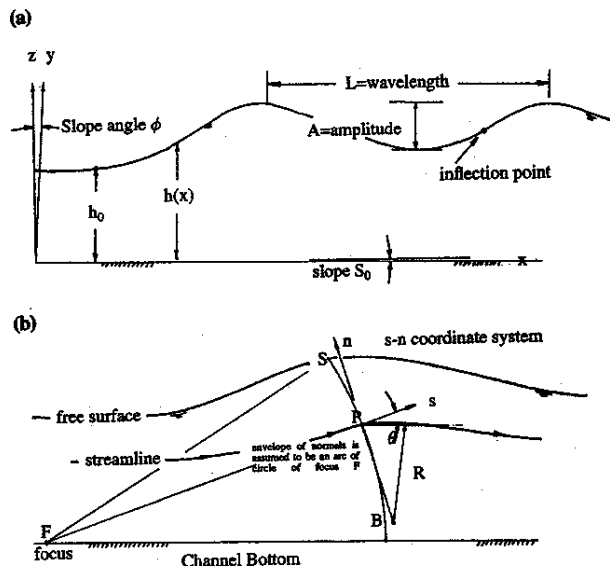


FIG. 9. (a) Undular Jump Geometry. System of Reference is Inclined at Angle ϕ with Respect to the Horizontal; (b) Streamline-Centered Coordinate System Used in Development of Inviscid Boussinesq Equation

$$\text{Energy} = \frac{\bar{E}}{h} = \cos \phi + \frac{U^2}{2gh} \left(1 + 2 \frac{\epsilon_0}{K+2} - \frac{\epsilon_1}{3} \right) + O(\epsilon^2) \quad (14)$$

and

$$\text{Momentum} = \frac{\bar{M}}{h^2} = \frac{\cos \phi}{2} + \frac{U^2}{gh} \left(1 + \frac{\epsilon_0}{K+2} - \frac{\epsilon_1}{3} \right) + O(\epsilon^2) \quad (15)$$

Modification of Inviscid Equations to Allow for Boundary Shear Effects

A velocity distribution was proposed by Prandtl (1927) and is today widely employed for the turbulent flow velocity distribution computations over smooth, flat surfaces. This distribution in its two equivalent forms for 2D flow with fully developed boundary layer ($\delta = h$) is

$$\frac{u}{U_{\max}} = \left(\frac{y}{h} \right)^N \quad (16a)$$

$$\frac{u}{U} = (1+N) \left(\frac{y}{h} \right)^N \quad (16b)$$

where U_{\max} = maximum longitudinal velocity; and U = mean longitudinal velocity. Later, Spence (1956) found that this type of velocity distribution fit the outer part of boundary layers developing under pressure gradients, but the inner part was better represented by the logarithmic velocity distribution. This agrees with the form of the outer velocity law as framed in Coles' law of the wake, discussed in the experimental results section.

The exponent *N* depends mainly on the pressure gradient of the flow, more weakly on the Reynolds number. Typical values of this parameter for flows with small pressure gradients are $N = 0.1$ to 0.15 for zero or positive pressures, rising to $N = 0.5$ for flows near separation in adverse pressure gradients. The right-hand side of (16b) may be considered a factor modifying the uniform inviscid flow distribution over a flat plate in parallel flow, where the exponent *N* tends to 0.

By analogy to this simple empirical law, the writers propose

to modify the inviscid streamline velocity distributions for wavy flow, Eq. (34) in Appendix I

$$V = V_s \exp \left[-\frac{\epsilon_0}{K+1} (1 - \eta^{K+1}) \right] + O(\epsilon^2) \quad \left(\eta = \frac{y}{h} \right)$$

to read

$$V = V_s \eta^N \exp \left[-\frac{\epsilon_0}{K+1} (1 - \eta^{K+1}) \right] + O(\epsilon^2) \quad (17)$$

By following steps similar to those detailed in Appendix I, one may derive from this basic equation the corresponding expressions for the longitudinal and transversal velocities, u and v , and the pressure p :

$$\text{Longitudinal velocity } u = \frac{u}{U} = (1+N)\eta^N \left[1 - \frac{\epsilon_0}{K+1} \cdot \left(\frac{1+N}{K+2+N} - \eta^{K+1} \right) - \frac{\epsilon_1}{2} \left(\frac{1+N}{3+N} + \eta^2 \right) \right] + O(\epsilon^2) \quad (18)$$

$$\text{Transversal velocity } v = \frac{v}{U} = (1+N)\eta^{1+N} \sqrt{\epsilon_1} \eta \left[1 - \frac{\epsilon_0}{K+1} \cdot \left(\frac{1+N}{K+2+N} - \eta^{K+1} \right) - \frac{\epsilon_1}{2} \left(\frac{1+N}{3+N} \right) \right] + O(\epsilon^2) \quad (19)$$

$$\text{Pressure } p = \frac{p}{\gamma h} = \cos \varphi (1 - \eta) + \frac{\epsilon_0(1+N)^2}{K+2N+1} \frac{U^2}{gh} (1 - \eta^{K+2N+1}) + O(\epsilon^2) \quad (20)$$

The Boussinesq equations corresponding to these velocity and pressure distributions can now be developed. (Here β = momentum correction coefficient, defined in Appendix IV. Notation.)

$$\text{Energy } = \frac{\bar{E}}{h} = \cos \varphi + \beta \frac{U^2}{2gh} \left\{ 1 + \frac{2\epsilon_0}{K+2+2N} \cdot \left[1 + N \left(2 + \frac{2N}{K+2+N} \right) \right] - \epsilon_1 \left(\frac{1+N}{3+N} \right) \right\} + O(\epsilon^2) \quad (21)$$

$$\text{Momentum } = \frac{\bar{M}}{h^2} = \frac{\cos \varphi}{2} + \beta \frac{U^2}{gh} \left\{ 1 + \epsilon_0 \left[\left(\frac{2}{K+N+2} - \frac{1-2N}{K+2+2N} \right) - \epsilon_1 \left(\frac{N+1}{N+3} \right) \right] \right\} + O(\epsilon^2) \quad (22)$$

The variation of the mean energy and momentum with distance x are assumed to be represented by the usual relations valid for quasi-parallel flow.

$$\frac{d\bar{E}}{dx} = S_0 - S_f; \quad \frac{d\bar{M}}{dx} = h(S_0 - S_f) \quad (23a,b)$$

In these relations S_f = gradient of energy line; and S_0 = bottom slope.

Integration of Boussinesq Equations, Calculation of Energy, and Momentum Change in Regions with Significant Pressure Gradient

One may use the extended energy equation (23a) to calculate the surface profile of the undular jump. This computation is complicated by the peculiar characteristics of the boundary layer development in the undular jump. Considering the profile between the upstream section and the first crest [Fig. 9(a)], one can see that the boundary layer in this zone has an adverse pressure gradient, and for the initial Froude numbers greater than 1.2 shock waves originating from the side walls of the

channel will be present. The experimental values of the transversal velocity distribution exponent N in (17) increase in magnitude in this region from about $N = 0.12$ at the section upstream to $N = 0.5$ at the crest. These are typical conditions for boundary layers approaching or reaching separation. As discussed in the previous section, the effect of boundary-layer thickening (if the upstream flow was undeveloped) and the onset of the shock waves on the sidewalls led to a considerable increase in the effective drag on the channel boundary, with the consequent reduction in the longitudinal energy and momentum. The combination of these two effects is particularly evident in the region before the first crest. Beyond this point the local Froude number decreases to well below its original upstream value, with the result that the drag-enhancing effect of the shock waves is much diminished.

The calculation of the frictional effects under the undular jump is a fairly complex problem. There are, in fact, very few studies of open-channel flow friction and velocity distribution with nonuniform characteristics. The recent work of Kironoto and Graf (1994, 1995), Song and Graf (1996), and Dunbabin (1996) are most noteworthy exceptions. However, the degree of flow nonuniformity in experiments by Graf and coworkers is much smaller than that encountered in the undular jump (as seen in the value of the Coles wake parameter Π in Fig. 6), so not a great deal of information from these studies can be incorporated in the present calculation of the friction characteristics of the flow under the undular jump. The most promising solution seems to be the application of a method used in the calculation of boundary layers with pressure gradients.

Among the wide variety of available methods, the extremely simple method developed by Furuya and Nakamura (1968) has been shown (Kline et al. 1968) to provide good results under a variety of pressure gradients. The method is attractive in the context of the present investigation, because it also uses as its basis the power law for velocity distribution in the wall region of the flow. Furuya and Nakamura showed that this replacement of the more widely accepted logarithmic velocity distribution works well provided that the boundary layer is not too close to separation, or what would be equivalent, that the shape parameter $H = \delta_*/\theta$ is kept below 2. In this relation δ_* = displacement thickness; and θ = momentum thickness of the boundary layer. This limitation constrains the applicability of the method, limiting the initial Froude number to a value of $F_0 \leq 1.4$.

In comparison with other methods, the Furuya and Nakamura's method appears exceptionally attractive because it requires only two very simple inputs: the value of the parameters θ and $C_f = (f/8)(U/U_{max})^2$ at the starting point of the calculations. Also, the structure of the method is such that it can be easily incorporated into the step-by-step numerical calculation using the extended energy equation. In contrast, other boundary-layer calculation procedures may require data that is impossible or inconvenient to supply for engineering computations such as integral parameters related to turbulence, entrainment parameters, or the dissipation integral.

It may be noted that Furuya and Nakamura's method also has a disadvantage: The calculation of the nondimensional friction parameter C_f under the undular jump has the added complication of a spatially oscillating but time-steady pressure field. Under this circumstance, the boundary layer needs some time to adjust to the pressure field—its "history" is important—and simple methods such as the one advocated here might not have enough adjustable parameters to adequately reflect this condition. However, because few, if any, boundary-layer computational methods have been tested under these exacting conditions, the Furuya and Nakamura method's advantages of simplicity of programming and good performance outweigh the possible disadvantages. Some details of the method are shown in Appendix II.

Another limitation of the application of the method is that the initial Froude number should be one with at best incipient formation of shock waves, since shock waves' contribution to the energy dissipation is not taken into account in the integration of the Boussinesq equations. These limitations restrict the application of Furuya and Nakamura's method of calculation of boundary friction to undular jumps of types A and those in the lower part of the B bracket.

Numerical Integration of the Extended Energy Equation

The system of energy conservation equations, (21) and (23a), was integrated numerically using Hamming's third order method (Hamming 1962) to determine the profile $h = h(x)$ of the undular jump. The boundary conditions for this case were set as follows: For a given initial Froude number F_0 , the initial depth h_0 of the supercritical flow was calculated from the expression $h_0/y_c = F_0^{-2/3}$, and the initial surface slope of the flow was set to an arbitrary positive value of $h' = 0.001$ to 0.01 to reflect the perturbation of the supercritical flow by the downstream control. It was found that the numerical magnitude of the starting value for h' had negligible effect on subsequent results—different choices of h' only slightly altered the distance between the upstream section and the first crest of the profile, while the depths and wavelengths remained unaltered. An integration using the momentum equation gave substantially similar results.

The relation between the exponent N of the power and the friction factor of the channel for a zero pressure gradient or small negative pressure gradient has been discussed by Chen (1990), who deduced from a simple integration of the velocity profile that

$$N = \frac{1}{\kappa} \sqrt{\frac{f}{8}} \quad (24)$$

where $\kappa =$ Von Karman's constant, with a magnitude close to 0.4. The measured values of f in Chanson's (1993) experiments indicate that N has an initial value close to 0.125 in most experiments.

RESULTS FROM THEORETICAL MODEL OF FLOW

It must be noted that the characteristics of the undular jumps are strongly dependent on the slope and roughness of the channel. Therefore, one must be very careful in comparing experiments from diverse sources, where the rate of change of momentum and energy may have been quite different. To present

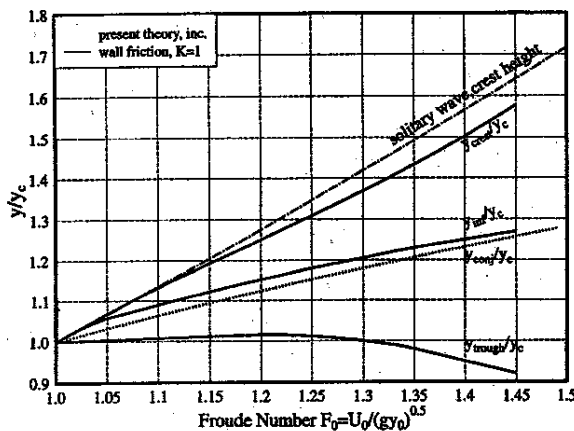


FIG. 10. Depths at First Crest, Inflection Point, and First Trough as Functions of Froude Number Calculated from Present Theory for Condition of Constant Downstream Energy or Momentum (Equilibrium Undular Jumps)

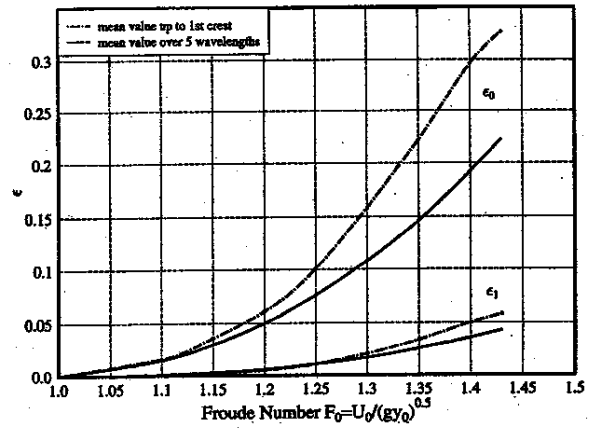


FIG. 11. Mean Values of Parameters ϵ_0 and ϵ_1 as Functions of Upstream Froude Number. These Establish Limit of Theory Validity, which is $F_0 = 1.4$, Approximately. Parameter $K = 1$ in this Calculation

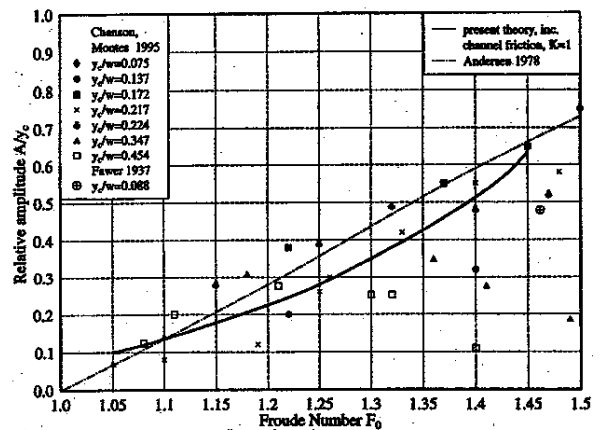


FIG. 12. Amplitude of First Undulation, for Constant Energy and $K = 1.0$. Comparison with Andersen's (1978) Theory

the main theoretical results it is convenient to define an ideal situation where the slope of the channel is such that the energy (or momentum) increases very slowly or remains constant in the region beyond the first crest. A decrease of either E or M beyond certain limits will collapse the numerical calculations, because no flows are possible below a value of E/y_c or M/y_c equal to 1.5. Some geometrical characteristics for the undular jump in terms of the initial Froude number for this idealized condition are given in Fig. 10, which describes the calculated depths at the first crest, first trough, and inflection point. As a comparison, the crest depth for the solitary wave (Boussinesq 1871) and for the conjugate depth of the conventional hydraulic jump have been added. The height of the first crest is close to the height of the solitary wave for smaller Froude numbers; the same similarity can be found between the inflection point depth and the conjugate depth of the normal hydraulic jump (Fig. 11).

Fig. 12 details the variation of the first-wave amplitude and Fig. 13 details that of the first wavelength. Both figures include a comparison with data from recent experiments and with the expressions suggested by Fawer (1973) and Andersen (1978). It may be noted that the theoretical expression for the amplitude seems to constitute a limit toward which the experiments tend as the aspect ratio of the flow tends to zero.

Limitation of Theory

The main assumption in the derivation of the theoretical model was that the curvature and slope were moderate, so that

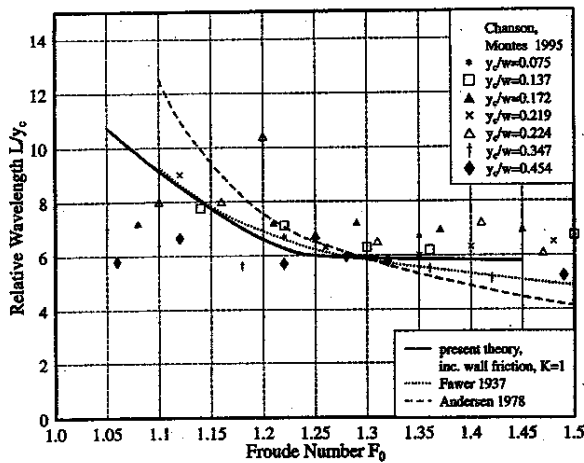


FIG. 13. Wavelength of First Undulation, for Constant Energy and $K = 1.0$. Comparison with Fawer's (1937) and Andersen's (1978) Theories and Present Experimental Data

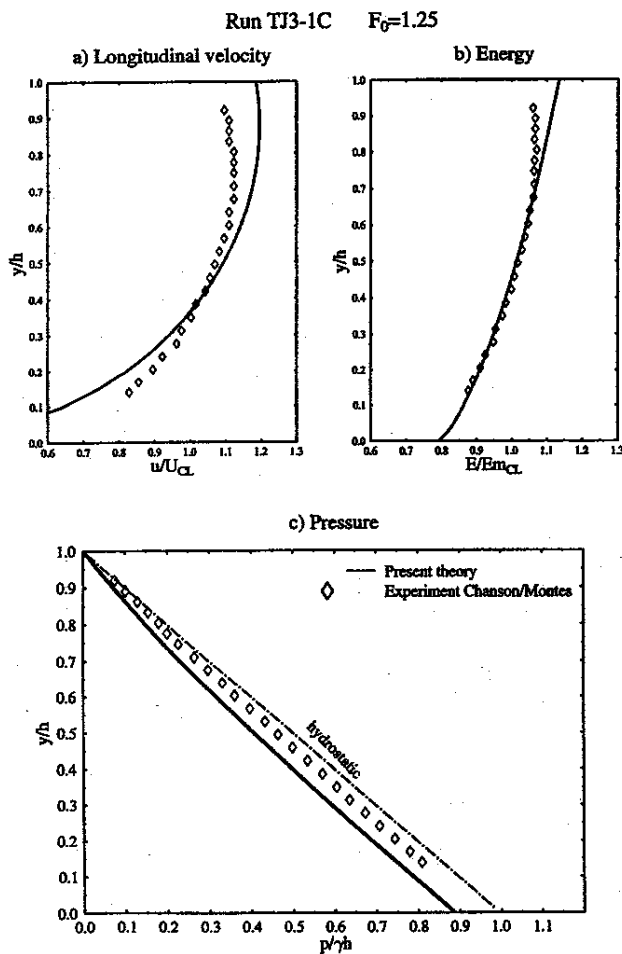


FIG. 14. Comparison of Data of Chanson (1995), Run TJ3, $F_0 = 1.25$ with Centerline Velocity, Energy, and Pressure Distribution Computed from Present Theory ($K = 1$). Location: under First Crest

the squares and higher powers of the parameters ϵ_0 and ϵ_1 could be taken as small in comparison with unity. From Fig. 12 it can be seen that the mean value of the curvature parameter $= 0.3$ when $F_0 = 1.4$. Its square is then much smaller than unity. The mean value of the slope parameter ϵ_1 remains smaller still and is less significant. This limit, $F_0 < 1.4$, is also close to the value at which the waves at the first crest

break, a limit that depends mainly on the aspect ratio, y_c/W , of the channel. For an infinitely wide channel this limit is close to $F_0 = 2$, but a value representative of the present experiments is closer to $F_0 = 1.4$. It is possible that the validity of the theory extends slightly beyond this value, since outside a narrow region around the crests of the undular jump the curvature is well below the limit of 0.3. The present theory also shows that at an initial Froude number of approximately 1.65, the surface velocity at the crest becomes a negative, incipient condition for the formation of a surface roller.

Figs. 14–17 contain a comparison with the measured centerline velocity, energy, and pressure distributions. Figs. 14 and 15 describe the conditions of run TJ1 (initial Froude number $F_0 = 1.27$) for the first crest and first trough locations. Figs. 16 and 17 portray these results at the same sections for run TJ7 (initial Froude number 1.48). In this comparison, the exponent K in (11) has been taken equal to 1.0. Numerical experimentation showed little difference in the output for values of K ranging from 0.5 to 2. It is evident from the results of Figs. 13–16 that the agreement between theory and experiments deteriorates as Froude numbers approach and exceed 1.5, as was to be expected considering the assumptions of moderate curvature and two-dimensionality made in the derivation of the theory.

CONCLUSIONS

Additional experiments to supplement the relatively meager collection of data have been performed and disclose the geo-

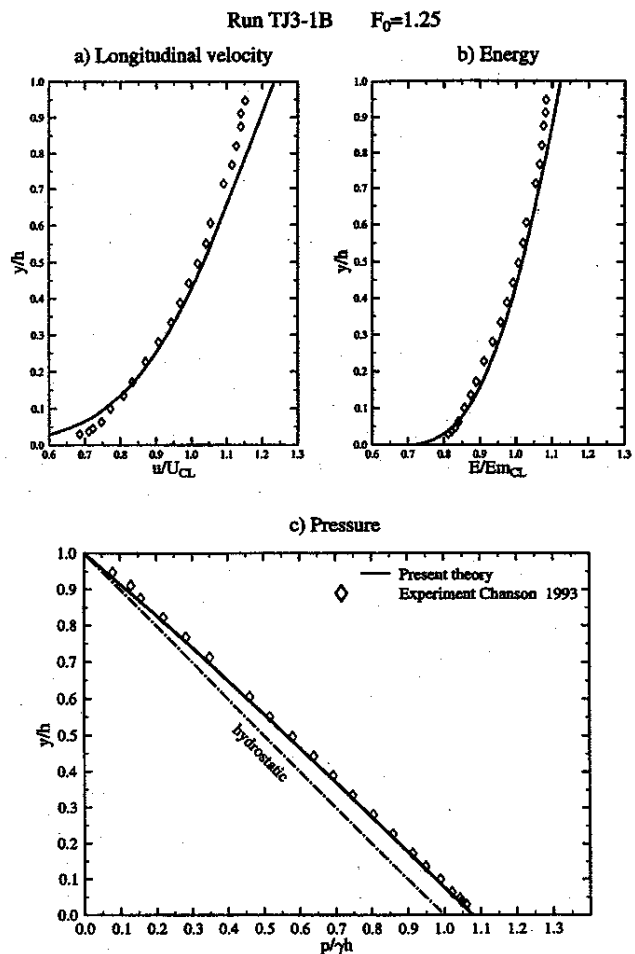


FIG. 15. Comparison of Data of Chanson (1995), Run TJ3, $F_0 = 1.25$ with Centerline Velocity, Energy, and Pressure Distribution Computed from Present Theory ($K = 1.0$). Location: under First Trough

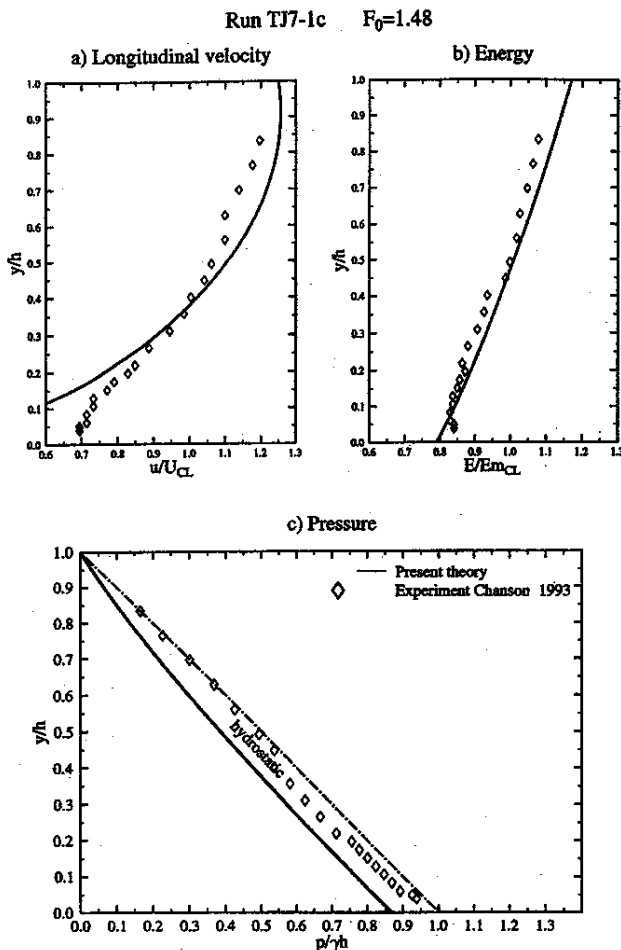


FIG. 16. Comparison of Data of Chanson (1995), Run TJ7, $F_0 = 1.48$ with Centerline Velocity, Energy, and Pressure Distribution Computed from Present Theory ($K = 1.0$). Location: under First Crest

metrical and kinematical characteristics of the undular jump. These experiments confirm the three-dimensional aspects of the undular jump, differentiating it from the similar phenomenon of the undular bore, a traveling train of cnoidal waves with which it shares some external characteristics. The undular jump shows strong side-wall effects, caused by the rapid growth of the wall boundary layer, and the formation of shock waves. The mechanism of shock-wave formation is explained in terms of wall boundary layer separation. The interaction of wall boundary layers with the shock waves is considerable even with a channel width to flow depth ratio of 7:1. The consequence is a marked rearrangement, with respect to a two-dimensional flow, of the transversal depth profile and velocity distribution, as well as other features of this phenomenon. In particular, one may observe a noticeable increase in the centerline discharge.

The velocity distribution in the region before the first crest is shown to contain a strong wake component, the magnitude of which is linked to the level of the adverse pressure gradient. These profiles are quite similar to those in boundary layers nearing separation and point to the wide variation of bottom shear between the beginning and the crest section of the boundary layer.

A two-dimensional Boussinesq equation modified for boundary shear effects was developed to predict the major features of the undular jump at F_0 less than 1.4 and the dependence of the jump characteristics on the local values of slope and roughness of the channel. The model presented here is

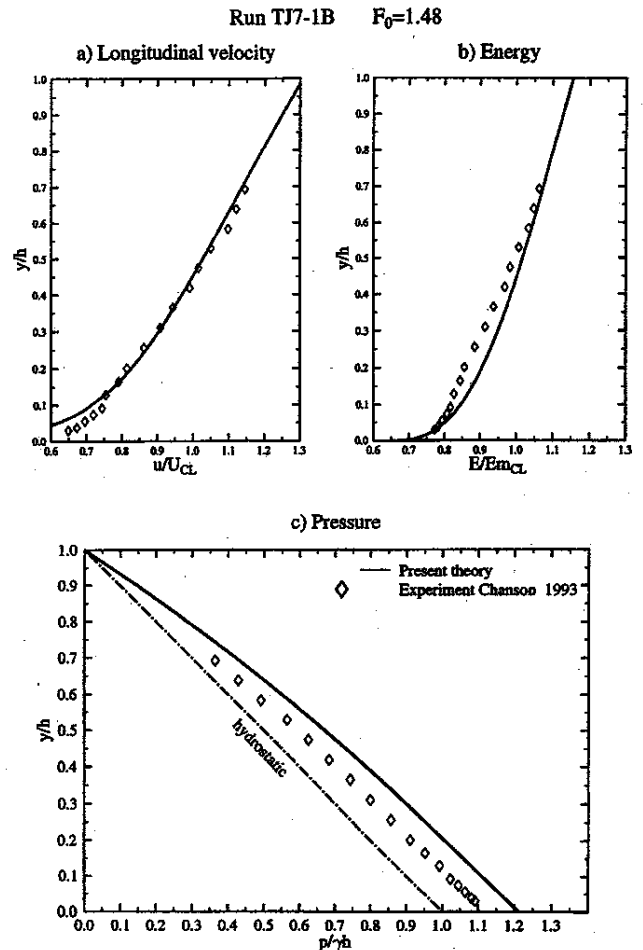


FIG. 17. Comparison of Data of Chanson (1995), Run TJ7, $F_0 = 1.48$ with Centerline Velocity, Energy, and Pressure Distribution Computed from Present Theory ($K = 1.0$). Location: under First Trough

restricted to moderate curvatures by the needs for mathematical simplicity and is able to predict with fair accuracy the depth variation and the influence of the surface curvature and slope on the velocity, energy, and pressure distributions. The theory also predicts the wavelength and amplitude of the undular jump, up to its limit of validity, which is restricted to type A jumps and the lower range of type B jumps.

It would be difficult to justify a more complex two-dimensional model in light of the surface perturbations caused by the oblique waves and the wave-breaking at crests at Froude numbers greater than 1.4. It is hoped that future work in this subject can be extended to a more realistic three-dimensional model, where special attention is given to the shock-wave generation process and to quantifying the energy dissipation associated with the oblique jumps.

APPENDIX I. DEVELOPMENT OF INVISCID BOUSSINESQ EQUATION

A streamline centered s - n system of reference is defined in Fig. 9(b). According to Rouse (1938), the inviscid flow equations of momentum conservation in this system are

$$V \frac{\partial V}{\partial s} = \frac{1}{\rho} \frac{\partial p}{\partial s} - g \frac{\partial z}{\partial s} \quad (25)$$

$$\frac{V^2}{R} = \frac{1}{\rho} \frac{\partial p}{\partial n} - g \frac{\partial z}{\partial n} \quad (26)$$

where V = streamline velocity; and R = local radius of curvature. Integrating (25) along a streamline gives the well-known result

$$H(n) = \frac{V^2}{2} + \frac{p}{\rho} + gz \quad (27)$$

For an irrotational flow the energy, $H(n)$, is constant. Eliminating the pressure gradient between (25) and (26), one obtains

$$\frac{1}{V} \frac{\partial V}{\partial n} = -\frac{1}{R} \quad (28)$$

Integrating (28) along the arc PS yields

$$\ln \left(\frac{V}{V_s} \right) = \int_n^{n_s} \frac{dn}{R} \quad (29)$$

where n_s and n are the arcs SB and PB in Fig. 9(b). Cartesian coordinates x and y are usually preferred, so the element of arc dn is replaced by its equivalent, $-dy/\cos \theta$.

$$\ln \left(\frac{V}{V_s} \right) = - \int_y^h \frac{dy}{R \cos \theta} \quad (30)$$

To proceed further, it is necessary to resort to some assumption regarding the variation of the radius of curvature R with the depth y . An assumption similar to that of Fawer (1937) links these variables by the relation

$$\frac{1}{R \cos \theta} = \frac{1}{R_b \cos \theta_b} + \left(\frac{1}{R_s \cos \theta_s} - \frac{1}{R_b \cos \theta_b} \right) \eta^K \quad (31)$$

where $\eta = y/h$. This relation provides a continuous variation between the boundary values of the radius of curvature. The subscripts b and s refer to bottom and surface conditions and K is a positive constant of the order of unity. If the bottom is flat (31) simplifies to

$$\frac{1}{R \cos \theta} = \frac{1}{R_s \cos \theta_s} \eta^K \quad (32)$$

Substituting (32) into (30) and integrating, the streamline velocity V is

$$V = V_s \exp \left[- \frac{1}{K+1} \frac{h}{R_s \cos \theta_s} (1 - \eta^{K+1}) \right] \quad (33)$$

As $\tan \theta_s = h'$ and $R_s = (1 + h'^2)^{1/2}/h'$, (33) is equivalent to

$$V = V_s \exp \left[- \frac{\epsilon_0}{K+1} (1 - \eta^{K+1}) \right] \quad (34)$$

where the parameter ϵ_0 stands for $hh''/(1 + h'^2)$ a term closely related to the relative curvature of the surface.

To obtain the longitudinal and transversal components of the velocity, the variation of the angle of inclination θ with y is now defined by assuming, as Boussinesq did, that the arc BS [Fig. 9(b)] can be taken to be an arc of circle; then all the tangents to the streamlines meet at a common point, F . Simple geometry shows that the angle θ is specified by

$$\sin \theta = \sin \theta_s \left(\frac{y}{h} \right) = \sqrt{\epsilon_1} \frac{y}{h}, \quad \cos \theta = \sqrt{1 - \epsilon_1 \left(\frac{y}{h} \right)^2} \quad (35a,b)$$

Here $\epsilon_1 = h'^2/(1 + h'^2)$.

The longitudinal velocity $u = V \cos \theta$ is now obtained by combining (34) and (35b). The resulting expression is approximated by expanding in series the exponential and square root functions that appear in these equations and neglecting the term $O(\epsilon^2)$. This is equivalent to assuming that the curvature is moderate everywhere.

$$u = V_s \left(1 - \frac{\epsilon_0}{K+1} (1 - \eta^{K+1}) - \frac{\epsilon_1}{2} \eta^2 \right) + O(\epsilon^2) \quad (36)$$

The velocity, v , to the same order of approximation, is

$$v = V \sin \theta = V_s \sqrt{\epsilon_1} \eta \left[1 - \frac{\epsilon_0}{K+1} (1 - \eta^K) \right] + O(\epsilon^2) \quad (37)$$

The mean horizontal velocity, $U = q/h$, is now

$$U = \frac{1}{n_s} \int_0^{n_s} V dn = \int_0^h V \frac{dy}{\cos \theta} = V_s \left(1 - \frac{\epsilon_0}{K+2} + \frac{\epsilon_1}{6} \right) + O(\epsilon^2) \quad (38)$$

Variable V_s in terms of U to same order is

$$V_s = U \left(1 + \frac{\epsilon_0}{K+2} - \frac{\epsilon_1}{6} \right) + O(\epsilon^2) \quad (39)$$

Then the ratio u/U is defined by

$$\frac{u}{U} = \left\{ 1 - \frac{\epsilon_0}{K+1} \left[\frac{1}{(K+2)} - \eta^{K+1} \right] - \frac{\epsilon_1}{6} (3\eta^2 + 1) \right\} + O(\epsilon^2) \quad (40)$$

and v/U is

$$\frac{v}{U} = \sqrt{\epsilon_1} \eta \left\{ 1 - \frac{\epsilon_0}{K+1} \left[\frac{1}{(K+2)} - \eta^{K+1} \right] - \frac{\epsilon_1}{6} \right\} + O(\epsilon^2) \quad (41)$$

The last expression is of higher order of approximation than (40).

Pressure Distribution

The variation of p along the arc PS [Fig. 9(b)] follows from the integration of (26) with the boundary condition that $p = 0$ at the surface. In Cartesian coordinates

$$p = \gamma(h - y) \cos \varphi + \rho \int_y^h \frac{V^2}{R \cos \theta} dy \quad (42)$$

By inserting in (42) the approximations for the radius of curvature and V , one obtains

$$\frac{p}{\gamma h} = (1 - \eta) \cos \varphi + \frac{U^2}{gh} \left(\frac{\epsilon_0}{K+1} \right) (1 - \eta^{K+1}) + O(\epsilon^2) \quad (43)$$

Extended Energy and Momentum Equations

The mean energy \bar{E} is the average through depth. The momentum \bar{M} of the flow represents the longitudinal momentum plus pressure force in that direction

$$\text{Energy} = \bar{E} = \frac{1}{h} \int_0^h E dy = \frac{1}{h} \int_0^h \left(y \cos \varphi + \frac{p}{\gamma} + \frac{V^2}{2g} \right) dy \quad (44a)$$

$$\text{Momentum} = \bar{M} = \int_0^{n_s} \left(\frac{u}{g} V + \frac{p \cos \theta}{\gamma} \right) dn \quad (44b)$$

Substitution of the equations (34), (40), and (41) for the streamline velocity, longitudinal and mean longitudinal velocity, and pressure into (44a) and (44b) gives

$$\bar{E} = h \cos \varphi + \frac{U^2}{2g} \left[1 + \frac{\epsilon_0}{K+2} - \frac{\epsilon_1}{3} \right] + O(\epsilon^2) \quad (45)$$

and

$$\bar{M} = \frac{h^2}{2} + \frac{U^2}{g} \left[1 + \frac{\epsilon_0}{K+2} \right] + O(\epsilon^2) \quad (46)$$

These equations, as could be expected from the similarity

of their basic assumptions, are almost identical to those suggested by Serre (1953), Matthew (1963), and Hager and Hutter (1984) if the curvature exponent K is taken equal to 1, but the degree of approximation in terms of the curvature and slope parameters is clearly stated.

APPENDIX II. FURUYA AND NAKAMURA'S METHOD FOR CALCULATION OF BOUNDARY LAYER'S FRICTIONAL EFFECTS

This method is a momentum integral method, supplemented by an equation for the momentum thickness within the boundary layer. It has been slightly modified to suit the characteristics of a free-surface flow with rather large adverse pressure gradients. The thickness of the boundary layer in this application has been assumed to be equal to the depth of the flow; therefore, the flow at the beginning of the jump must be well-developed. The velocity profile between the solid boundary and the momentum thickness $\theta < h$ is assumed to follow a power law similar to that in (16a). Furuya and Nakamura use as a special parameter the ratio of the boundary layer velocity at $y = \theta$ to the maximum velocity at $y = h$. This parameter, $K = u_\theta/U_\infty$, is related here to the shape parameter $H = \delta_*/\theta$ of the boundary layer by the empirical relation

$$H = [1.3 + 1.3(0.7 - K) + 3(0.7 - K)^2]^{0.667} \quad (47)$$

Ludwig and Tillman (1949) developed a useful expression for the skin friction coefficient $(C_f/2) = (\tau_w/\rho U_\infty^2)$, which incorporates the shape parameter H

$$\frac{C_f}{2} = 0.123 R_0^{-0.268} \times 10^{-0.678H}; \quad R_0 = \frac{U_\infty \theta}{\nu} \quad (48)$$

Here U_∞ is the maximum velocity within the cross section. The procedure of calculation with this method consists of integrating step by step the differential equations for θ and K . The first is Von Karman's momentum integral equation

$$\frac{d\theta}{dx} = -\frac{\theta}{U_\infty} \frac{dU_\infty}{dx} (H + 2) + \frac{C_f}{2} \quad (49)$$

The second is a transport equation for the shape parameter K , derived by integrating the x momentum equation from $y = 0$ to $y = \theta$.

$$\frac{dK}{dx} = 1.46 \frac{1 - K^2}{(K + A)\theta R_0^{0.25}} [\Gamma + 0.118(0.67 - K)] \quad (50)$$

Here $\Gamma = (\theta/U_\infty)(dU_\infty/dx)R_0^{0.25}$ is Buri's shape factor (Schlichting 1960). The empirical coefficient A has been given here a value of $A = 1.5$ to provide additional computational stability. The maximum velocity $U_\infty \approx (1 + N)q/h$, where N is the exponent in the power law velocity distribution, given by Spence's (1956) relation $N = (H - 1)/2$.

APPENDIX III. REFERENCES

Andersen, V. M. (1978). "Undular hydraulic jump." *J. Hydr. Div., ASCE*, 104(8), 1185-1188.

Bakhmeteff, B. A., and Matzke, A. E. (1936). "The hydraulic jump in terms of dynamic similarity." *Trans. ASCE*, 101, 630-647.

Bazin, H. (1865). "Recherches expérimentales sur la propagation des ondes [Experimental research on wave propagation]." *Mémoires présentés par divers Savants à l'Académie des Sciences*, Paris, France, 19, 495 (in French).

Binnie, A. M. and Orkney, J. C. (1955). "Experiments on the flow of water from a reservoir through an open horizontal channel. II: The formation of hydraulic jump." *Proc., Royal Soc. of London, Series A*, 230, 1181, 237-246.

Boussinesq, J. V. (1871). "Sur le mouvement permanent varié de l'eau dans les tuyaux de conduite et dans les canaux découverts [On the steady varied flow of water in conduits and open channels]." *Comptes*

Rendus des Séances de l'Académie des Sciences, Paris, France, 73, 101-105 (in French).

Boussinesq, J. V. (1877). "Essai sur la théorie des eaux courantes [Essay on the theory of water flow]." *Mémoires présentés par divers Savants à l'Académie des Sciences*, Paris, France, Series 3, 23(1), suppl. 24, 1-680 (in French).

Chanson, H. (1993). "Characteristics of undular hydraulic jumps." *Research Report No. CE146*, Dept. of Civ. Engrg., Univ. of Queensland, Australia.

Chanson, H. (1995). "Flow characteristics of undular hydraulic jumps: Comparison with near-critical flows." *Report CH45/95*, Dept. of Civ. Engrg., Univ. of Queensland, Australia.

Chanson, H., and Montes J. S. (1995). "Characteristics of undular hydraulic jumps. 1: Experimental apparatus and flow patterns." *J. Hydr. Engrg.*, ASCE, 122(2), 129-144.

Chen, C. L. (1990). "Unified theory on power laws for flow resistance." *J. Hydr. Engrg.*, ASCE, 117(3), 371-389.

Coles, D. E., and Hirst, E. A. (eds.) (1968). *Proc., Computation of Turbulent Boundary Layers, AFOSR-IFP-Stanford Conf.*, Vol. 2.

Darcy, H., and Bazin, H. (1865). "Recherches hydrauliques [Hydraulic research]." *Imprimerie Impériale, Parties 1e et 2e*, Paris, France (in French).

Dunbabin, R. (1996). "Velocity distributions within an undular hydraulic jump." Honors thesis, Dept. of Civ. and Mech. Engrg., Univ. of Tasmania, Hobart, Tasmania, Australia.

Engelund, F., and Munch-Petersen, J. (1953). "Steady flow in contracted and expanded rectangular channels: Some considerations concerning the shape of the water surface." *J. La Houille Blanche*, 8, Aug/Sept., 464-474.

Fawer, C. (1937). "Etudes des quelques écoulements permanents a filets courbes," Thesis, Université de Lausanne, Lausanne, France.

Furuya, Y., and Nakamura, I. (1968). "A semi-integrated momentum method for the auxiliary equation." *Proc., Computation of Turbulent Boundary Layers AFOSR-IFP-Stanford Conf.*, Vol. 1, 235-246.

Hager, W. H., and Hutter, K. (1984). "On pseudo-uniform flow in open channel hydraulics." *Acta Mechanica*, 53, 183-200.

Hamming, R. W. (1962). *Numerical methods for scientists and engineers*. McGraw-Hill Inc., New York, N.Y.

Hilton, W. F. (1952). *High speed aerodynamics*. Longmans, Green and Co., London, U.K.

Ippen, A. T. (1951). "Mechanics of supercritical flow." *Trans. ASCE*, 116, 268-295.

Ippen, A. T., and Harleman, R. F. (1956). "Verification of theory for oblique standing waves." *Trans. ASCE*, 121, 678-694.

Kironoto, B. A., and Graf, W. H. (1994). "Turbulence characteristics in rough, open channel flow." *Proc., Inst. of Civ. Engrs., Water, Maritime, and Energy Div.*, Vol. 106, 333-344.

Kironoto, B. A., and Graf, W. H. (1995). "Turbulence characteristics in rough, non-uniform open channel flow." *Proc., Inst. of Civ. Engrs., Water, Maritime, and Energy Div.*, Vol. 112, 336-348.

Kline, S. J. (ed.) (1968). *Proc., Computation of Turbulent Boundary Layers, AFOSR-IFP Stanford Conf.*, Vol. 1.

Liggett, J. A. (1994). *Fluid mechanics*. McGraw-Hill Inc., New York, N.Y.

Lindus, K. (1996). "Investigation of the formation of lateral shock-waves in undular hydraulic jumps." Honors thesis, Dept. of Civ. and Mech. Engrg., Univ. of Tasmania, Hobart, Tasmania, Australia.

Ludwig, H., and Tillman, W. (1949). "Untersuchungen über die Wand-schubspannungen in turbulenten Reibungsschichten [Investigation of wall shear-stress in turbulent flow]." *Ingenieur Archiv*, 17, 288-299 (in German).

Matthew, G. D. (1963). "On the influence of curvature, surface tension and viscosity on flow over round crested weirs." *Proc., Inst. of Civ. Engrs.*, London U.K., 25, 511-524.

Prandtl, L. (1927). "Über den Reibungswiderstand strömender Luft [On the frictional resistance of airflow]." *Ergebnisse AVA Göttingen*, 3rd Series, Nos. 1-5 (in German).

Rouse, H. (1938). *Fluid mechanics for hydraulic engineers*. McGraw-Hill Book Co. Inc., New York, N.Y.

Ryabenko, A. A. (1990). "Conditions favorable to the existence of an undulating jump." *Gidrotechnicheskoe Stroitel'stvo*, translated in *Hydrotechnical Constructions*, Plenum Publishing Corp., New York, N.Y., 762-770.

Schlichting, H. (1960). *Boundary layer theory*, J. Kestin, translator. McGraw-Hill Inc., New York, N.Y.

Serre, F. (Dec. 1953). "Contribution à l'Etude des Ecoulements Permanents et Variables dans les Canaux. [Contribution to the study of permanent and non-permanent flows in channels]." *J. la houille blanche*, 830-872 (in French).

- Spence, D. A. (1956). "The development of the boundary layer." *J. Aeronautical Sciences*, 22, 3-15.
- Yasuda, Y., Ohtsu, I. O., and Gotou, H. (1993). "A few experiments on the undular hydraulic jump." *Proc., 48th Annual Meeting JSCE, JSCE, Japan*, 2-159 (in Japanese).

APPENDIX IV. NOTATION

The following symbols are used in this paper:

- A = wave amplitude (m);
 D = drag force (N);
 E = specific energy (m);
 \bar{E} = mean specific energy (m);
 $(E_m)_{CL}$ = mean specific energy (m) on centerline;
 F_r = Froude number defined as $F = q/\sqrt{gh^3}$;
 F_0 = upstream Froude number $F_0 = q/\sqrt{gh_0^3}$;
 F_r^* = Froude number characterizing appearance of a small "cockscomb" roller at top of first wave crest;
 f = Darcy friction factor;
 g = gravitational constant: $g = 9.803 \text{ m/s}^2$ in Hobart, Australia;
 H = total head (m);
 H = shape parameter of boundary layer, $H = \delta^*/\theta$;
 h = local surface depth (m), measured perpendicular to channel;
 h_0 = flow depth (m), measured immediately upstream of hydraulic jump;
 h' = dh/dx ;
 h'' = d^2h/dx^2 ;
 K = exponent in streamline radius of curvature distribution;
 L = wave length (m);
 \bar{M} = specific momentum of flow (kg/s^2);
 M_A = Mach number in compressible flow;
 N = exponent of power law velocity distribution;
 n = length of arc normal to a streamline (m);
 p = pressure (Pa);
 Q = discharge (m^3/s);
 q = discharge per unit width (m^2/s);
 $(q)_{CL}$ = discharge per unit width (m^2/s) on centerline;
 R = local radius of curvature of streamline (m);
 R = Reynold's number;
 s = length of arc along streamline (m);
 S_0 = bottom slope;
 S_f = slope of energy line;
 u = longitudinal velocity, parallel to channel bottom (m/s);
 U_* = shear velocity $u_* = \sqrt{\tau_b/\rho}$, (m/s);
 U = mean flow velocity, $U = Q/A$ (m/s);
 U_{max} = maximum longitudinal velocity on centerline (m/s);
 U_{CL} = mean longitudinal velocity on centerline (m/s);

- V = velocity along streamline (m/s);
 W = channel width (m);
 x = distance along channel bottom (m);
 y = distance from bed measured perpendicular to channel surface (m);
 y_c = critical flow depth (m) for a rectangular channel: $y_c = \sqrt[3]{q^2/g}$;
 z = bed elevation from datum (m) taken positive upward;
 β = Boussinesq momentum correction coefficient $\beta = \int u^2 dA/U^2 A$; also dimensionless pressure gradient defined by $\beta = (gh/u_*^2)(dh/dx)$;
 ΔE = variation in the specific energy of flow (m);
 ΔH = energy dissipation at center line (m);
 Δx = increment in x direction (m);
 δ = boundary layer thickness (m);
 δ^* = boundary layer separation thickness = $\int_0^\infty (1 - u/U_\infty) dy$;
 K = Von Karman's velocity distribution parameter;
 η = dimensionless vertical coordinate $\eta = y/h$;
 θ = angle of inclination of streamline with channel (deg.); also momentum thickness in boundary layer = $\int_0^\infty u/U_\infty [1 - (u/U_\infty)] dy$;
 θ^* = angle between lateral shock waves and side walls at start of lateral shock waves;
 γ = ρg (N/m^3);
 Π = amplitude parameter in Coles' law of the wake;
 ρ = water density (kg/m^3);
 τ_b = bottom shear stress (N/m^2); and
 ϕ = channel slope angle measured with respect to the horizontal (deg.).

Subscripts

- b = channel bottom;
 B = wave trough;
 C = wave crest;
 CL = on flume centerline;
 i = at inflexion point;
 s = on surface;
 0 = flow conditions upstream of hydraulic jump;
 1 = flow conditions downstream of hydraulic jump; and
 $*$ = start of lateral shock waves.

Abbreviations

- BL = boundary layer;
 SW = location of start of lateral shock waves;
 U/S = upstream flow;
 1C = first wave crest; and
 1B = first wave trough.